Magnetostatic coupling of 90° domain walls in Fe$_{19}$Ni$_{81}$/Cu/Co trilayers

J Kurde[1,4]**, J Miguel**[1,5]**, D Bayer**[2]**, J Sánchez-Barriga**[3]**,
F Kronast**[3]**, M Aeschlimann**[2]**, H A Dürr**[3,6]** and W Kuch**[1]

[1] Institut für Experimentalphysik, Freie Universität Berlin, Arnimallee 14,
14195 Berlin-Dahlem, Germany
[2] Department of Physics and Research Center OPTIMAS,
University of Kaiserslautern, 67663 Kaiserslautern, Germany
[3] Helmholtz-Zentrum Berlin für Materialien und Energie,
Elektronenspeicherring BESSY II, Albert-Einstein-Strasse 15, 12489 Berlin,
Germany
E-mail: julia.kurde@fu-berlin.de

Abstract. The magnetic interlayer coupling of Fe$_{19}$Ni$_{81}$/Cu/Co trilayered microstructures has been studied by means of x-ray magnetic circular dichroism in combination with photoelectron emission microscopy (XMCD-PEEM). We find that a parallel coupling between magnetic domains coexists with a non-parallel coupling between magnetic domain walls (DWs) of each ferromagnetic layer. We attribute the non-parallel coupling of the two magnetic layers to local magnetic stray fields arising at DWs in the magnetically harder Co layer. In the magnetically softer FeNi layer, non-ordinary DWs, such as 270° and 90° DWs with overshoot of the magnetization either inwards or outwards relative to the turning direction of the Co magnetization, are identified. Micromagnetic simulations reveal that in the absence of magnetic anisotropy, both types of overshooting DWs are energetically equivalent. However, if a uniaxial in-plane anisotropy is present, the relative orientation of the DWs with respect to the anisotropy axis determines which of these DWs is energetically favorable.

---

[4] Author to whom any correspondence should be addressed.

[5] Present address: Diamond Light Source Ltd, I06, Harwell Science and Innovation Campus, Didcot, Oxfordshire, OX11 0DE, UK.

[6] Present address: SLAC National Accelerator Laboratory, 2575 Sand Hill Road, Menlo Park, CA 94025, USA.

Contents

1. Introduction

Since the first demonstration of indirect exchange coupling between the magnetization of two ferromagnetic (FM) layers separated by a non-magnetic spacer layer in 1986 [1], much attention has been paid to its oscillatory character [2]–[5]. However, magnetostatic interactions due to stray fields arising at rough FM/spacer interfaces or domain walls (DWs) can also lead to strong coupling effects between FM layers, as had already been described in the 1960s [6]–[8]. These early findings were followed by various experimental and theoretical projects concerning magnetostatic coupling effects at interfaces [9, 10], DWs [11]–[16] or vortex cores [17]. In 180° Néel walls, the magnetization turns opposite in the two FM layers to reduce the magnetostatic energy without the cost of wall energy [7]. On the other hand, in decoupled films, 360° DWs or other kinds of quasi-walls can be found [8, 12, 14], where the magnetization on both sides of the wall points in the same direction in one of the two FM layers. These walls cost wall energy without being necessary in this FM layer, which demonstrates the strength of the stray fields created by DWs. Not so frequently discussed are DWs in coupled films with angles smaller than 180° in one layer, where an opposite turn of the magnetization in the other FM layer would lead to walls with more than 180°. In this work, we focus on 90° Néel walls, which typically appear in rectangular microstructures of low anisotropy magnetic materials, where the magnetization is preferentially in a flux-closure domain state. We show the influence stray fields at 90° Néel walls in the magnetically harder layer have on Néel walls in the magnetically softer layer by comparing experimental observations to micromagnetic simulations. These results contribute to our understanding of stray field effects at DWs and demonstrate the diversity of magnetic coupling phenomena.

Trilayered $Fe_{19}Ni_{81}$/Cu/Co microstructures with sizes 5×5, 5×15 and $10 \times 10\,\mu m^2$ and thicknesses $t_{FeNi} = 4$ nm, $t_{Co} = 15$ nm and $t_{Cu} = 1.5$, 2 and 3 nm are investigated. The Cu layer acts as a non-magnetic spacer. In the following, $Fe_{19}Ni_{81}$ will be referred to as FeNi. To examine the magnetic domain configuration of the different FM layers independently, we have used x-ray magnetic circular dichroism in combination with photoelectron emission microscopy (XMCD–PEEM) [18, 19]. This technique provides the lateral resolution and the element-selective magnetic contrast, which are essential for the study of magnetic micron-sized systems consisting of different layers. In the FM/spacer/FM trilayer system presented here, the coupling of the two FM layers is dominated by Néel coupling due to their polycrystallinity, interface roughness, and the relatively large spacer thicknesses at which indirect exchange coupling contributions are insignificant. Magnetic domains of the two FM layers are thus
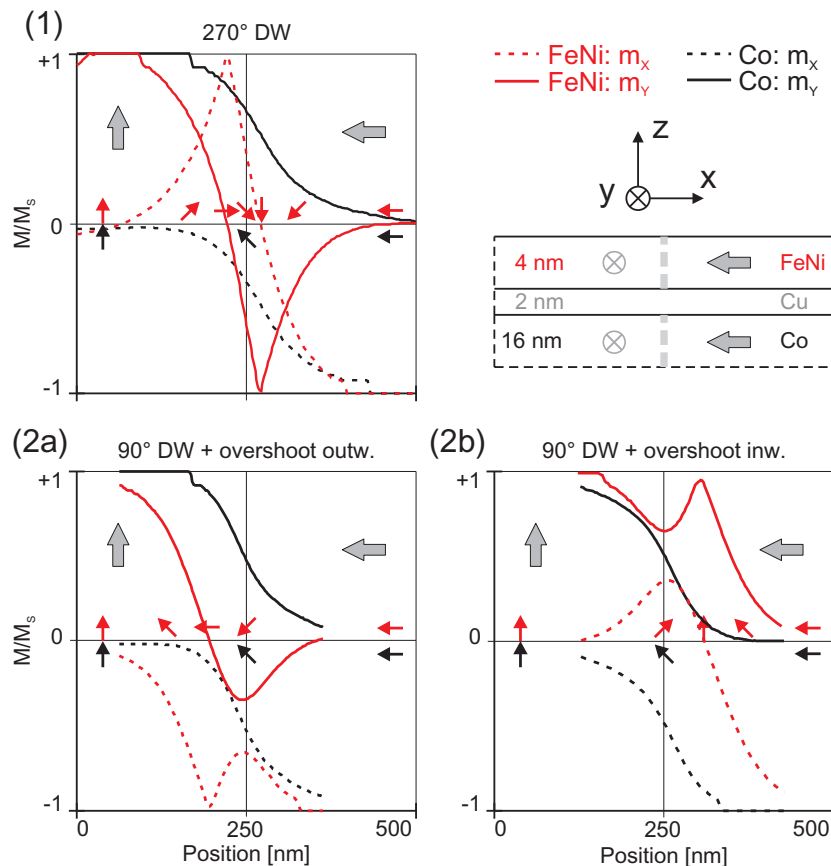
Figure 1. Line profiles of the x-(dashed lines) and y-(solid lines)components of the magnetization vector of the FeNi (red) and the Co layer (black) across non-parallel coupled 90° DWs taken from micromagnetic simulations, illustrating three possibilities: 270° DWs (1) and 90° DWs with overshoot of the magnetization outwards (2a) and inwards (2b) relative to the turning direction of the Co magnetization. Gray arrows indicate magnetization in the two domains, and red and black arrows indicate magnetization across the DWs in the FeNi and the Co layer, respectively.

aligned in parallel. However, this is no longer valid at the DWs, where a non-parallel coupling is present for spacer thicknesses larger than 1.5 nm. We will discuss three different kinds of non-ordinary 90° DWs in the FeNi layer, allowing an opposite or near-opposite orientation of the magnetization as compared to the Co layer: 270° DWs (case (1)) and 90° DWs with overshoot of the magnetization outwards (case (2a)) or inwards (case (2b)) relative to the turning direction of the Co magnetization. These possibilities are sketched in figure 1, where red and black arrows and lines indicate the magnetization in the soft FeNi and hard Co layer, respectively. The x- and y-components of the magnetization are taken from micromagnetic simulations (see below). Comparing the magnetization components in the FeNi layer in the three cases, in case (1) both the x- and y-components reverse, while in cases (2a) and (2b) only the x- or the y-component changes sign. This will later serve us as a criterion to distinguish case (1) from case (2a) or (2b) in the experimental images. Note that, due to symmetry reasons, cases (2a) and (2b) are degenerate in energy as long as no uniaxial magnetic anisotropy is present.

IOP Institute of Physics **Φ** DEUTSCHE PHYSIKALISCHE GESELLSCHAFT

2. Experimental details

Electron-beam lithography was employed to define the microstructures on top of a GaAs substrate. Subsequently, magnetic layers were deposited by magnetron sputtering in an Ar$^+$ pressure of 1.5×10^{-3} mbar with a base pressure better than 3×10^{-8} mbar. During deposition, a magnetic field of 100 mT was applied to introduce a small magnetic in-plane anisotropy in the Co layer. XMCD images were acquired with an Elmitec PEEM instrument at the UE49-PGMa microfocus beamline at BESSY II in Berlin. With a grazing incidence of $16°$, this instrument is particularly suited to the study of samples with in-plane magnetization. A lateral resolution of about 80 nm was achieved in the measurements presented in this work. Element selectivity was obtained by tuning the photon energy of the incoming x-ray beam to the Fe L_3 absorption edge at 707 eV for the FeNi layer and to the Co L_3 absorption edge at 778 eV for the Co layer. The magnetic contrast was obtained by calculating the asymmetry, given by the difference in intensity between two images taken with opposite circular photon helicity and normalized by the sum.

Micromagnetic simulations were performed with the OOMMF micromagnetic simulator (http://math.nist.gov/oommf/), which solves the Landau–Lifshitz–Gilbert equation [20, 21] with the so-called finite differences method for a three-dimensional (3D) cubic mesh. We used a discretization cell size of $5 \times 5 \times 2$ nm^3 and the usual parameters for saturation magnetization M_S and exchange constant A of FeNi ($M_S = 796$ kA m^{-1}, $A = 13$ pJ m^{-1}) and Co ($M_S = 1400$ kA m^{-1}, $A = 30$ pJ m^{-1}). The damping coefficient α was set to a relatively large value of 0.5 for quasi static conditions. The simulations were run until the change in angle of the magnetization between two successive iterations was less than 0.01 deg ns^{-1} across all spins. A parallel coupling between the two FM layers was introduced by the *two-surface exchange* term provided in the OOMMF package, using a bilinear surface exchange coefficient $\sigma = 0.36 \times 10^{-4}$ J m^{-2}. This corresponds to a Néel coupling for a spacer thickness of 2 nm, with an interface roughness amplitude of 1 nm and a period of 10–20 nm, which is reasonable for our samples. Magnetic anisotropy was not considered for simulations of the square-shaped structures. However, for the rectangular structures, a small in-plane anisotropy field of 20 kA m^{-1} along the long edge of the structure was introduced to better adapt the simulation to the experiment.

3. Results and discussion

3.1. Experiment

The spacer thickness t_{Cu} influences the ratio between the parallel Néel coupling and the antiparallel coupling via stray fields at DWs, because of the different decay lengths. In figure 2, the magnetization of microstructures with $t_{Cu} = 1.5$ nm (a), $t_{Cu} = 2$ nm (b) and $t_{Cu} = 3$ nm (c) is compared. Color-coded XMCD–PEEM images probing the y-component of the magnetization are shown for the FeNi layer (top) and the Co layer (bottom). Blue and red contrast corresponds to the negative and positive y-components of the magnetization, respectively. Consequently, $180°$ DWs separate blue from red domains, while $90°$ DWs are found between blue or red and white domains. The magnetization within domains is indicated by gray arrows (figure 2, bottom). With $t_{Cu} = 1.5$ nm, the two FM layers are coupled in parallel. Some $180°$ DWs in the FeNi layer already indicate a competition between parallel and stray field coupling, visible by
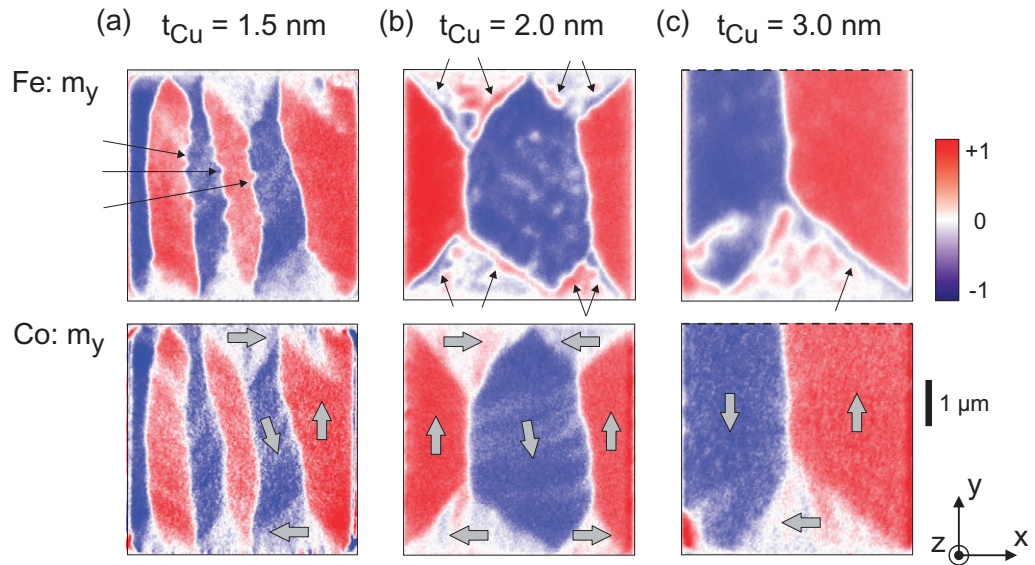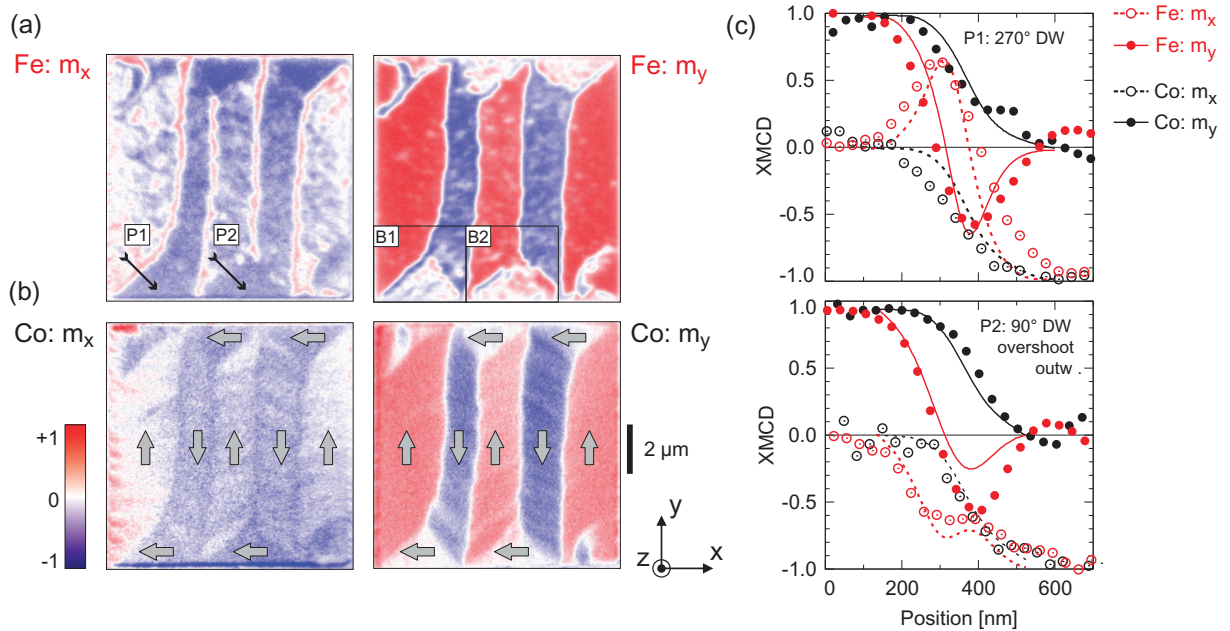
Figure 2. Color-coded XMCD–PEEM images of trilayer microstructures with (a) $t_{Cu} = 1.5$ nm, (b) $t_{Cu} = 2$ nm and (c) $t_{Cu} = 3$ nm probing the y-component of the magnetization in the FeNi (top) and the Co layer (bottom). Blue and red contrast corresponds to the negative and positive y-components of the magnetization, respectively. In the FeNi layer, an undulated shape of 180° DWs is visible for $t_{Cu} = 1.5$ nm (black arrows in (a)); and a non-parallel coupling in 90° DWs is observed for $t_{Cu} = 2$ and 3 nm (black arrows in (b) and (c)).

their undulated shape (black arrows in figure 2(a)). With $t_{Cu} = 2$ and 3 nm, the opposite contrast appears at 90° DWs in the FeNi layer: blue between a red and a white domain, and red between a blue and a white domain (black arrows in figures 2(b) and (c)). Thus, the two FM layers clearly exhibit a non-parallel coupling in the vicinity of 90° DWs. Note that in figure 2(c) only the lower part of the $5 \times 15 \, \mu m^2$ structure is shown. Both microstructures, one with $t_{Cu} = 2$ nm and the other with $t_{Cu} = 3$ nm, exhibit the same kind of non-parallel 90° DW coupling. Once the Néel coupling field drops below the stray field at DWs between $t_{Cu} = 1.5$ and 2 nm, a non-parallel alignment of the magnetization in the two FM layers arises. However, there is no visible difference between $t_{Cu} = 2$ and 3 nm.

The domains in the FeNi layer in figures 2(b) and (c) have a blotchy texture compared to the longitudinal ripple structure that is present in the other images. The ripple structure is typical of polycrystalline high-anisotropy films [22]. We attribute the blotchy texture to the fact that the ripples in the Co layer are a variation of magnetization direction, which creates small but quite irregular stray fields. These stray fields influence the magnetization of the FeNi layer. The different domain sizes in the three microstructures shown in figure 2 are random and not related to the Cu thickness.

For a more detailed analysis of the DW coupling, structures with $t_{Cu} = 3$ nm were imaged in two different geometries, where the x-ray incidence, and accordingly the magnetic contrast, is along the x- and y-directions, respectively. This provides full information about the in-plane components of the magnetization, which is necessary for completely characterizing these types of DWs. The in-plane magnetization of a $10 \times 10 \, \mu m^2$ microstructure with $t_{Cu} = 3$ nm is shown

Figure 3. Color-coded XMCD–PEEM images of a $10 \times 10 \, \mu m^2$ microstructure with $t_{Cu} = 3 \, nm$, probing the x- and y-components of the magnetization in (a) the FeNi and (b) the Co layer. Blue and red contrast corresponds to the negative and positive x- and y-components of the magnetization, respectively. (c) Wall profiles of two different DWs, as indicated by arrows in (a). Symbols represent the experimental wall profiles, while lines show the simulated profiles from figure 1 convoluted with a Gaussian corresponding to the experimental resolution. The experimental error for the vertical axis corresponding to noise in the XMCD images can be estimated as ± 0.15.

in figure 3 for the FeNi layer (a) and the Co layer (b). The color code of the XMCD–PEEM images is the same as used in figure 2. The magnetization is in a flux-closure multi-domain state, as indicated by gray arrows in figure 3(b). The magnetization in 180° DWs is oriented opposite in the two FM layers, as can be seen in the images probing the x-component of the magnetization, where they appear red in the FeNi layer and blue in the Co layer. In the image probing the y-component, on the other hand, a non-parallel alignment at 90° DWs can be found, e.g., in the regions indicated by the two boxes B1 and B2 in figure 3(a).

We have analyzed exemplary line profiles of two different types of non-parallel DWs, labeled as P1 and P2 and indicated by black arrows in figure 3(a). The magnetization components in both layers along these line profiles are given in figure 3(c). In both cases, the normalized x-component of the magnetization in the Co layer (black hollow circles) goes continuously from $m_x^{Co} = 0$ to -1, while the y-component (black solid circles) shows a similar change from $m_y^{Co} = +1$ to 0. Thus the magnetization in the Co layer turns continuously from the $+y$ to the $-x$ direction, as in ordinary 90° DWs. The situation is different for the FeNi layer. Here, in wall profile P1, the x-component (red hollow circles) starts at $m_x^{FeNi} = 0$ and ends at -1 as in the case of Co, but becomes positive in between. Similarly, the y-component (red solid circles) becomes negative as it evolves from $m_y^{FeNi} = +1$ to 0. Comparing

the experimental wall profiles P1 (figure 3(c), left) with the simulated ones (figure 1), they show a clear correspondence to the 270° DW. Note that to account for the experimental resolution, the simulated profiles were convoluted with a Gaussian with a half-width at half-maximum (HWHM) of 30 nm. The results of this convolution are represented by solid and dashed lines in figure 3(c). For wall profile P2, it can be seen how the y-component of the magnetization in the FeNi layer is very similar to the corresponding one in wall profile P1. In contrast, the x-component goes from $m_x^{\mathrm{FeNi}} = 0$ to -1 without changing its sign. Comparing again with the simulated wall profiles in figure 1, this type of DW can be identified as a 90° DW with overshoot of the magnetization outwards (case (2a) of figure 1). In general, good agreement between experiment and simulation is achieved. Note that the y-component of the FeNi layer in profile P2 has a deeper minimum in the experiment than in the simulation, indicating that the overshoot is larger in the experiment. The out-of-plane component M_z is considered to be zero in the experiment, which is confirmed by the micromagnetic simulations, where M_z turns out to be less than 10% of the saturation magnetization M_s.

Summarizing the above findings, in the experimental images we have identified two types of non-ordinary 90° DWs in the magnetically softer FeNi layer of a trilayered microstructure: (1) 270° DWs and (2) 90° DWs with an overshoot of the magnetization outwards relative to the turning direction of the Co magnetization. While DWs of type (1) give an opposite contrast in the x- and y-components, DWs of type (2) are mainly visible in the images probing the y-component of the magnetization.

3.2. Micromagnetic simulations

We have performed micromagnetic simulations for two different structure shapes: squared $1 \times 1\,\mu\mathrm{m}^2$ in a four-domain Landau state and rectangular $1 \times 2\,\mu\mathrm{m}^2$ in an elongated four-domain Landau state. The FM/spacer/FM trilayer system comprises 4 nm FeNi, 2 nm spacer and 16 nm Co. In all simulations, the magnetization of the Co layer was first relaxed separately, without the FeNi layer. The result was then used as the starting configuration for the relaxation of the complete trilayer. Since the Co layer stays rather unchanged during relaxation of the trilayer system, in the following we will focus on the effect of the stray field arising from the Co layer on the FeNi layer.

Simulations of the squared microstructure are shown in figure 4, where the magnetization $\mathbf{m} = \mathbf{M}/M_S$ of the FeNi layer (figure 4(a)) and of the separately relaxed Co layer (figure 4(c)) are shown together with the stray field $\mathbf{H}_{\mathrm{demag}}$ (figure 4(b)) calculated 4 nm above the Co layer, i.e. at the central plane of the FeNi layer. Color-coded x-, y- and z-components are represented from left to right. The stray field has significant intensities where the magnetization changes direction: in the DWs and at the vortex core in the center of the microstructure. Its direction at DWs is indicated by arrows in figure 4(b): magnetic charges lead to a stray field, which is oriented opposite to $\mathbf{M}$ in the Co layer. The result of the relaxation of the trilayer system for the FeNi layer, which was initially in the same Landau state as the Co layer, is represented in figure 4(a). The effect of the stray field is clearly visible at the corners of the structure. All four DWs are of type (2a) or (2b) (see figure 1). In the upper right corner of the structure, the magnetization turns with an overshoot inwards. In all other corners, it turns with an overshoot outwards, as found for the wall profile P2 in the experimental images. It is not clear *a priori* whether the relaxation will lead to DWs of type (2a) or (2b). In the initial configuration, the magnetization in the DWs is parallel in both layers but antiparallel to $\mathbf{H}_{\mathrm{demag}}$ in the FeNi layer.
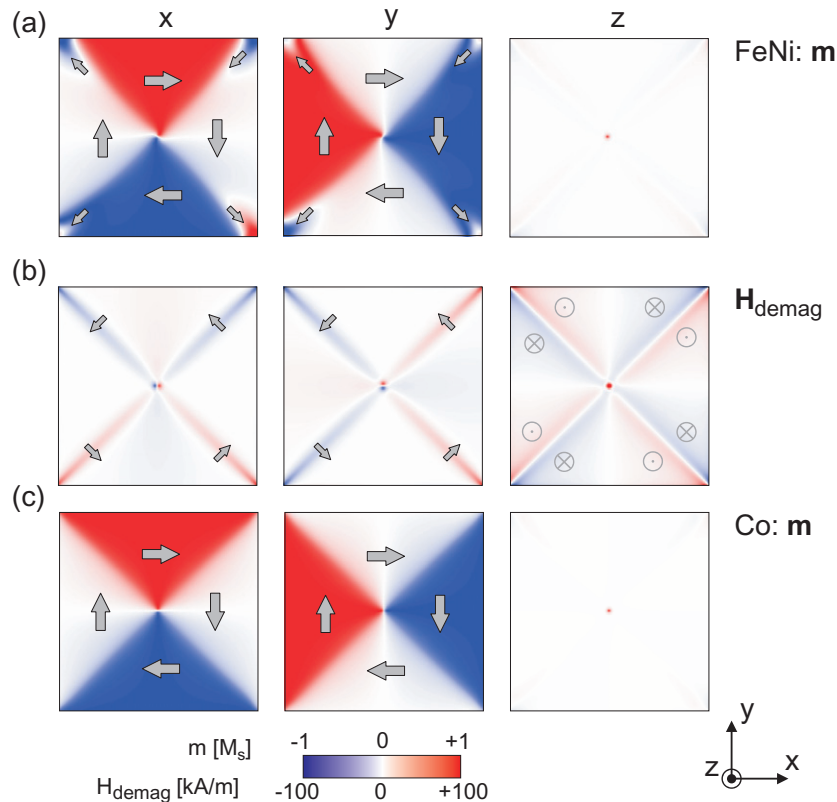
Figure 4. Simulation of a $1 \times 1\,\mu\mathrm{m}^2$ structure with Landau configuration. (a) Relaxed magnetization $\mathbf{m} = \mathbf{M}/M_s$ of the FeNi layer in the combined trilayer system, (b) stray field $\mathbf{H}_{\mathrm{demag}}$ 4 nm above the separate Co layer and (c) magnetization $\mathbf{m}$ of the separate Co layer.

This represents a symmetric maximum in energy and $\mathbf{M}$ can relax in any of the two directions. If this symmetry is broken by a small external field (1 mT) pointing either inwards or outwards along the DWs in the beginning of the relaxation process, all of the configurations with inwards or outwards overshoot of the magnetization for the four DWs can be created. Moreover, all of them have the same total energy in the case of a squared structure without anisotropy.

The main feature of the calculated Landau configuration is the vortex at the crossing point of the four DWs. Close to it, the four DWs join a circling magnetization. The in-plane amplitude of $\mathbf{H}_{\mathrm{demag}}$ is decreasing from the structure corners to the vortex core, and DWs of type (1) or type (2) cannot be maintained up to the joining point of the 90° DWs as it is found in the experiment. On the other hand, the experimental domain configuration, e.g. inside the two boxes B1 and B2 in figure 3(a), does not contain a vortex in the Co layer. Two 90° DWs rather join in a 180° DW. To account for that in the simulation, we extended the squared structure to a rectangular structure where the vortex core is not directly at the DW junction in the Co layer. Different initial magnetizations $\mathbf{M}_0^{\mathrm{FeNi}}$ for the FeNi layer were used, as shown for the lower half of the structure in figures 5(a)–(d). The upper half is point symmetric with respect to the center of the structure. The magnetization is given by big gray arrows in the domains and by small arrows in DWs: red for the FeNi layer and black for the Co layer. Figure 5(e) sketches the magnetization of the Co layer for the complete structure. In the experiment, a
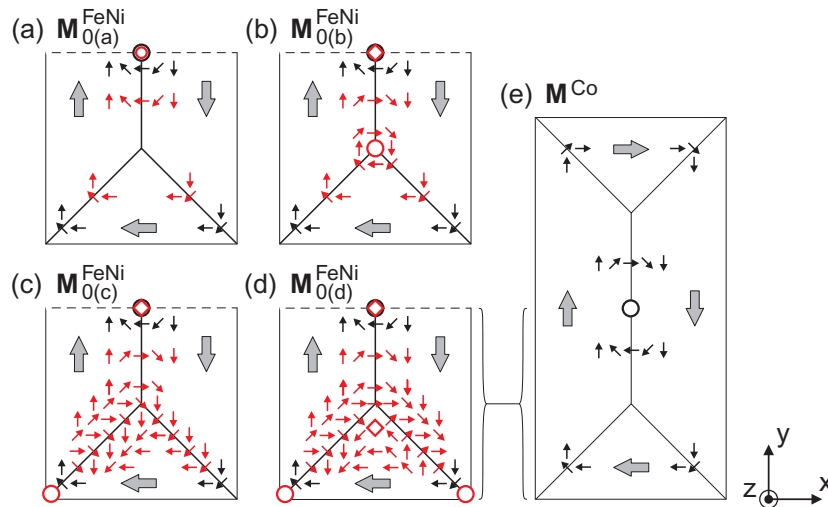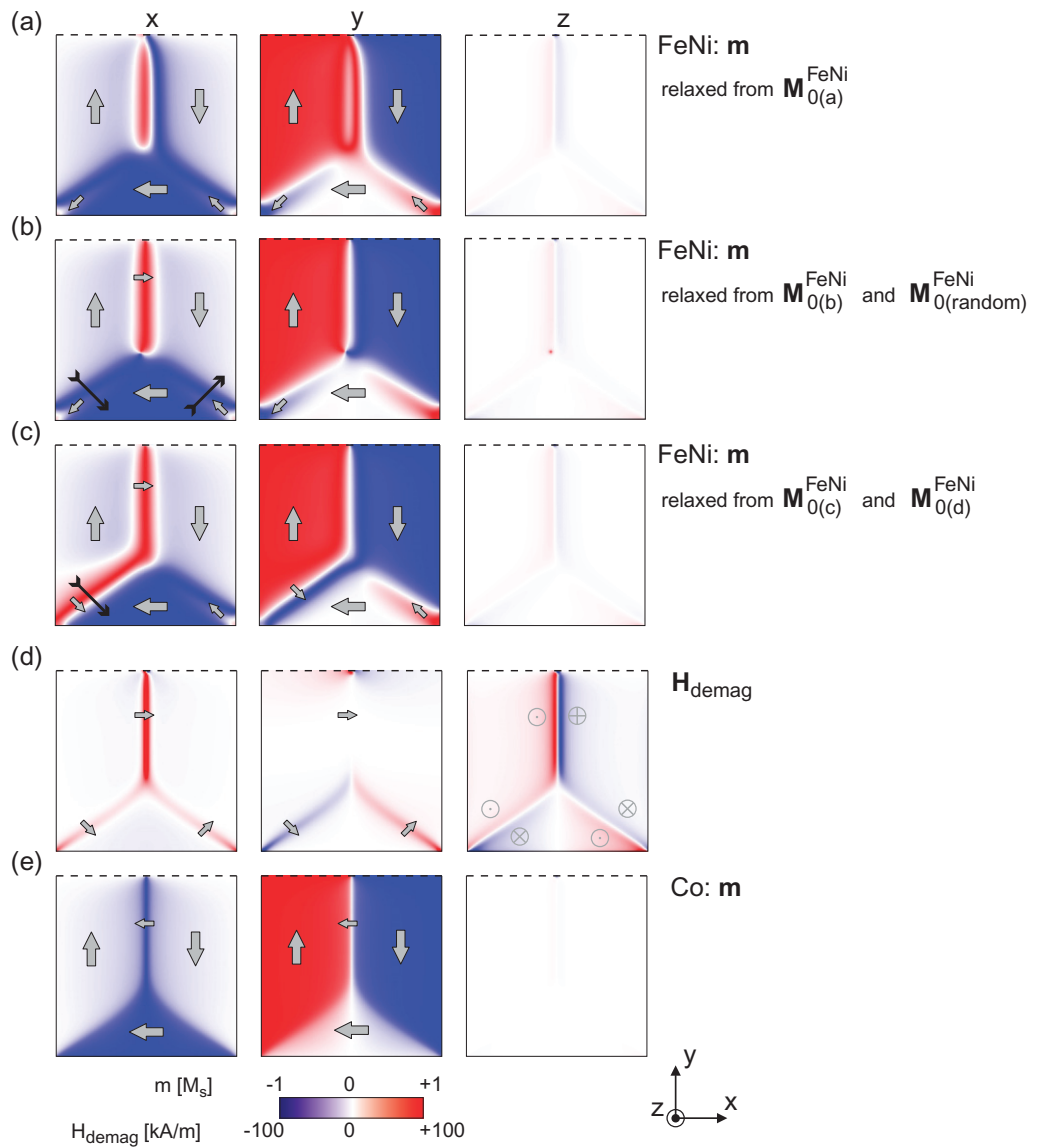
Figure 5. Sketch of the initial configurations of the magnetization of the FeNi layer for simulations of a $1 \times 2 \, \mu m^2$ structure. The magnetization is given by big gray arrows in the domains and by small arrows in DWs: red for the FeNi layer and black for the Co layer. (a) **M** is parallel in both layers, (b) **M** turns opposite in the 180° DWs of the two magnetic layers but parallel in the 90° DWs, (c) **M** turns opposite also in the left DW, creating 270° DWs in the FeNi layer, (d) two joining 270° DWs and (e) sketch of the Co magnetization in the complete microstructure. The circles and squares represent vortices and antivortices, respectively.

small in-plane anisotropy along the y-direction is present, which is now included in these simulations.

First, the initial magnetization for the FeNi layer was relaxed separately, so that the magnetization in both FM layers is mostly parallel (figure 5(a)). The result of the relaxation of the combined trilayer system is shown in figure 6(a). Figure 6(d) represents the stray field $\mathbf{H}_{demag}$ calculated 4 nm above the single Co layer and figure 6(e) the magnetization of the separately relaxed Co layer. In contrast to the vortex in the squared structure (figure 4), $\mathbf{H}_{demag}$ now features a smooth function of the position near the joining point of the two 90° DWs. Note that the wall profiles shown in figures 1 and 3(b) were obtained by line scans along the black arrows in figure 6(b) for DWs of type (2) and figure 6(c) for type (1) DWs. The FeNi layer exhibits after relaxation a 90° DW of type (2a) on the left and a 90° DW of type (2b) on the right (figure 6(a)), which can also be found in the experimental images (e.g. box B2 in figure 3(a)). The important effect of the magnetic anisotropy is that the 90° DWs do not divide the corner of the structure symmetrically any more, as in the case of the square structure. The angle between the DW and the long edge of the structure is larger. In consequence, the degeneracy between DWs of type (2a) and (2b) in the FeNi layer is now lifted. Domain walls that display an overshoot of the magnetization such that the magnetization component parallel to the anisotropy axis (y-axis in the present case) changes its sign are energetically favored. Hence, these DWs are mainly visible in the images showing the y-component of the magnetization. The same behavior is observed in the experimental images. For the 180° DW, however, the relaxation process ends up in an asymmetric solution, because the orientation of this wall is only partly reversed. If in the initial magnetization the 180° DW already has opposite

Figure 6. Relaxed magnetization of the lower half of the rectangular structure for different initial configurations $\mathbf{M}_0^{FeNi}$. (a) $\mathbf{M}_{0(a)}^{FeNi}$ as sketched in figures 5(a), (b) $\mathbf{M}_{0(b)}^{FeNi}$ as sketched in figure 5(b) or $\mathbf{M}_{0(random)}^{FeNi}$ and (c) $\mathbf{M}_{0(c)}^{FeNi}$ or $\mathbf{M}_{0(d)}^{FeNi}$ as sketched in figures 5(c) and (d), respectively. Black arrows indicate the positions at which the wall profiles shown in figures 1 and 3(c) are taken. (d) Stray field $\mathbf{H}_{demag}$ 4 nm above the separate Co layer; (e) relaxed magnetization of the separate Co layer. The x-, y- and z-components are shown from left to right.

magnetization orientations in the two FM layers (figure 5(b)), the relaxed magnetization of the FeNi layer (figure 6(b)) has the same kind of 90° DWs as before, but the 180° DW is now symmetric. The total energy is now lower: 7388 J m^{-3} versus 7655 J m^{-3}. If parallel oriented 90° DWs in both FM layers are lower in total energy than a 270° DW in the soft FM layer, it is very unlikely to go from one to the other by relaxation, since the total energy is mostly lowered

in each iteration. On the other hand, in the experimental images, DWs of type (1) are present in e.g. the lower left or upper right corner of the structure in figure 3(a). A random initial magnetization $\mathbf{M}_{0(\mathrm{random})}^{\mathrm{FeNi}}$ in the FeNi layer could allow the relaxation process to end up in a 270° DW. This is analogous to the deposition of the FeNi layer on top of a Co layer with a certain domain configuration, and therefore depicts a realistic configuration. The relaxation process, nevertheless, runs into the same solution with DWs of type (2a) and (2b) (figure 6(b)), as already obtained for $\mathbf{M}_{0(b)}^{\mathrm{FeNi}}$ (figure 5(b)). The experimental interface roughness and the statistical distribution of crystalline grains in the Co layer were not included in the simulations, which could be one reason why no 270° DWs evolve from $\mathbf{M}_{0(\mathrm{random})}^{\mathrm{FeNi}}$. It should also be mentioned that maybe 270° DWs are more easily formed if the magnetic domains are larger, or the DWs longer.

A 270° DW does not seem to correspond to a deep minimum in total energy. However, explicitly assuming a 270° DW in the initial magnetization (figure 5(c)), the relaxation process preserves it (figure 6(c)), proving that this configuration does represent a local minimum of the total energy. It also agrees nicely with the experiment (box B1 in figure 3(a)). In this case, the total energy of 7538 J m^{-3} is slightly higher than for the solution with two DWs of type (2), but still lower than for the solution with an asymmetric 180° DW. Finally, two joining 270° DWs (figure 5(d)) are considered. Comparing the four initial configurations in figures 5(a)–(d), in panel (a) there is no vortex at the DW junction, in panel (b) there is a vortex in the FeNi layer at the DW junction, in panel (c) this vortex is shifted to the end of the 270° DW at the lower left corner of the microstructure, and in panel (d) there are vortices in both lower corners of the microstructure and an antivortex in between, just below the DW junction. The fact that in figure 5(d) the antivortex does not lie on a line with the two vortices is already a hint that this configuration could be unstable. The relaxation process indeed eliminates one of the two 270° DWs by annihilation of the antivortex with one of the vortices. The result is again the same as obtained for $\mathbf{M}_{0(c)}^{\mathrm{FeNi}}$ (figure 5(c)) with only one 270° DW (figure 6(c)). In this context, note that in the experimental images, two joining 270° DWs are not observed.

Indirect magnetic coupling in thin magnetic multilayered structures is of considerable interest, particularly because of its importance in magnetoresistive or other kinds of magnetic storage devices. In single layer microstructures, where the magnetization is in a vortex state, two kinds of information could be stored: the sense of magnetization rotation around the vortex core (chirality c) and the magnetization orientation in the vortex core (polarity p), which is either up or down. In coupled trilayer microstructures, the relative orientations $c_1 c_2 = \pm 1$ and $p_1 p_2 = \pm 1$ of the individual layers provide further opportunities [17]. Our results show that in square-shaped trilayer microstructures with a four-domain closed-flux Landau state, one could think of additionally encoding one bit in each overshoot DW by its inwards or outwards orientation. For this purpose, it would be advantageous to optimize interface roughness and magnetic anisotropy towards a deep minimum in total energy for inwards and outwards overshoot DWs, without favoring one of the two. Efficient reading and writing of the stored information remains a challenge.

In future experiments, it will be interesting to compare the dynamic behavior of these DWs to those in single layer FeNi films [24] or stronger coupled trilayer structures [25]. The precession modes will depend on the wall type (1, 2a or 2b), and on the configuration at the joining point: two joining type (2) DWs, like in figure 6(b), or a type (1) DW joining a type (2) DW, like in figure 6(c).

IOP Institute of Physics Φ DEUTSCHE PHYSIKALISCHE GESELLSCHAFT

4. Conclusion

In summary, we have investigated the effects of stray fields and magnetic anisotropy in coupled FeNi/Cu/Co trilayered microstructures, especially in the vicinity of 90° DWs. Due to magnetostatic interlayer coupling, we found a non-parallel orientation of the magnetization of the two FM layers at 90° DWs for Cu thicknesses larger than 1.5 nm. This result clearly indicates that the DWs in the softer FeNi layer must be different from ordinary 90° DWs. From a comparison between the experimental findings and micromagnetic simulations, we have identified two different types of non-ordinary DWs that can be formed in the soft FM layer: (1) 270° DWs or (2) 90° DWs with an overshoot of the magnetization outwards or inwards relative to the turning direction of the Co magnetization. We have attributed the formation of these types of DWs to a reduction in the magnetostatic energy originating from the fringe field of the DWs in the magnetically harder FM layer. Micromagnetic simulations have also shown that without magnetic anisotropy, inwards or outwards DWs are energetically equivalent. However, if a uniaxial in-plane anisotropy field, as present in the experimental structures, is included in the simulation, the experimentally observed configuration is energetically favored.

Acknowledgments

References

[1] Grünberg P, Schreiber R, Pang Y, Brodsky M B and Sowers H 1986 *Phys. Rev. Lett.* **57** 2442
[2] Parkin S S P, More N and Roche K P 1990 *Phys. Rev. Lett.* **64** 2304
[3] Bruno P and Chappert C 1991 *Phys. Rev. Lett.* **67** 1602
[4] Unguris J, Celotta R J and Pierce D T 1994 *J. Appl. Phys.* **75** 6437
[5] Stiles M D 1999 *J. Magn. Magn. Mat.* **200** 322
[6] Néel L 1962 *Comptes. Rendus* **255** 1676
[7] Slonczewski J C 1966 *J. Appl. Phys.* **37** 1268
[8] Middelhoek S 1966 *J. Appl. Phys.* **37** 1276
[9] Schrag B B *et al* 2000 *Appl. Phys. Lett.* **77** 2373
[10] Kuch W, Chelaru L I, Offi F, Wang J, Kotsugi M and Kirschner J 2006 *Nat. Mater.* **5** 128
[11] Thomas L, Samant M G and Parkin S S P 2000 *Phys. Rev. Lett.* **84** 1816
[12] Schäfer R, Urban R, Ullmann D, Meyerheim H L, Heinrich B, Schultz L and Kirschner J 2002 *Phys. B* **65** 144405
[13] Kuch W, Chelaru L I, Fukumoto K, Porrati F, Offi F, Kotsugi M and Kirschner J 2003 *Phys. Rev. B* **67** 214403
[14] Vogel J *et al* 2005 *Phys. Rev. B* **72** 220402
[15] Vogel J, Cherifi S, Pizzini S, Romanens F, Camarero J, Petroff F, Heun S and Locatelli A 2007 *J. Phys.: Condens. Matter.* **19** 476204
[16] Berkov D V and Gorn N L 2008 *J. Appl. Phys.* **103** 053908
[17] Buchanan K S, Guslienko K Y, Choe S-B, Doran A, Scholl A, Bader S D and Novosad V 2005 *J. Appl. Phys.* **97** 10H503
[18] Stöhr J, Wu Y, Hermsmeier B D, Samant M G, Harp G R, Koranda S, Dunham D and Tonner B P 1993 *Science* **259** 658

[19] Kuch W, Frömter R, Gilles J, Hartmann D, Ziethen Ch, Schneider C M, Schönhense G, Swiech W and Kirschner J 1998 *Surf. Rev. Lett.* **5** 1241

[20] Landau L D and Lifshitz E M 1935 *Phys. Z. Sowietunion* **8** 153

[21] Brown W F Jr 1963 *Micromagnetics* (New York: Interscience, Wiley)

[22] Harte K J 1968 *J. Appl. Phys.* **39** 1503

[23] Hubert A and Schäfer R 2000 *Magnetic Domains: the Analysis of Magnetic Microstructures* (Berlin: Springer)

[24] Miguel J, Sánchez-Barriga J, Bayer D, Kurde J, Heitkamp B, Piantek M, Kronast F, Aeschlimann M, Dürr H A and Kuch W 2009 *J. Phys.: Condens. Matter.* **21** 496001

[25] Schneider C M, Kaiser A, Wiemann C, Tieg C and Cramm S 2010 *J. Electron. Spectrosc. Relat. Phenom.* **181** 159